Peter Renner
J. Mike Walker '66 Department of Mechanical Engineering,
Texas A&M University,
202 Spence Street,
College Station, TX 77843
e-mail: parenner@tamu.edu

Swarn Jha
J. Mike Walker '66 Department of Mechanical Engineering,
Texas A&M University,
202 Spence Street,
College Station, TX 77843
e-mail: swarn.jha14@tamu.edu

Yan Chen
Department of Materials Science & Engineering,
Texas A&M University,
College Station, TX 77843
e-mail: yanchen876@tamu.edu

Tariq Chagouri
Department of Petroleum Engineering,
Texas A&M University at Qatar,
Education City PO Box 23874,
Doha, Qatar
e-mail: tariq.chagouri@qatar.tamu.edu

Serge Kazadi
J. Mike Walker '66 Department of Mechanical Engineering,
Texas A&M University,
202 Spence Street,
College Station, TX 77843
e-mail: s_kazadi@tamu.edu

Mohamed Gharib
Department of Mechanical Engineering,
Texas A&M University at Qatar,
Education City PO Box 23874,
Doha, Qatar
e-mail: mohamed.gharib@qatar.tamu.edu

Hong Liang[1]
Mem. ASME
J. Mike Walker '66 Department of Mechanical Engineering,
Texas A&M University,
202 Spence Street,
College Station, TX 77843
e-mail: hliang@tamu.edu

Corrosion-Resistant Metal-Ceramic Composite Coatings for Tribological Applications

Effective design of corrosion-resistant coatings is critical for the protection of metals and alloys. Many state-of-the-art corrosion-resistant coatings are unable to satisfy the challenges in extreme environments for tribological applications, such as elevated or cryogenic temperatures, high mechanical loads and impacts, severe wear, chemical attack, or a combination of these. The nature of challenging conditions demands that coatings have high corrosion and wear resistance, sustained friction control, and maintain surface integrity. In this research, multi-performance metal-ceramic composite coatings were developed for applications in harsh environments. These coatings were developed with an easy to fabricate, low-cost, and safe procedure. The coating consisted of boron nitride, graphite, silicon carbide, and transition metals such as chromium or nickel using epoxy as vehicle and bonding agent. Salt spray (SS) corrosion tests showed that 1010 carbon steel (1/4 hard temper) substrates lost 20–100 × more mass than the coatings. The potentiodynamic polarization study showed better performance of the coatings by seven orders of magnitude in terms of corrosion relative to the substrate. Additionally, the corrosion rates of the coatings with Ni as an additive were five orders of magnitude lower than reported. The coefficient of friction (COF) of coatings was as low as 0.1, five to six times lower than that of epoxy and lower than a wide range of epoxy resin-based coatings found in literature. Coatings developed here exhibited potential in applications in challenging environments for tribological applications. [DOI: 10.1115/1.4052867]

Keywords: coatings, corrosion, dry friction, friction, scratching, surface properties and characterization, surface roughness and asperities

Introduction

Corrosion in metals and alloys is one of the major causes of material failure that leads to immense economic loss [1,2]. In electrochemical corrosion (EC), material loss is driven by chemical reactions which occur on the surface of the metal or alloy [1–3]. The severity, extent, and rate of corrosion are governed by several parameters such as the change in Gibbs free energy, Pilling-Bedworth ratio (P-B ratio), salinity, sulfate content, dissolved oxygen content, pH, and temperature [4–7]. Wear is one of the most common failures which can cause irreversible degradation and lead to failure of a material. It has been widely reported that tribotesting has been conducted on all types of materials and can be used to accurately analyze material surface performance and failure mechanisms [8–15]. While many methods of combatting surface failure exist [12,16,17], coatings developed for extreme environments enable improved tribological performance via

[1]Corresponding author.
Contributed by the Tribology Division of ASME for publication in the JOURNAL OF TRIBOLOGY. Manuscript received August 11, 2021; final manuscript received October 14, 2021; published online November 25, 2021. Assoc. Editor: Yi Zhu.

surface modification. As such, coatings allow for the use of cheap and mechanically competent materials such as carbon steel to be used in extreme environments.

Polymer-based coatings have used in corrosion protection [18–23]. For instance, polymers that are used for surface functionalization of nanomaterials include Dextran, Starch, Chitosan, PVP, PVA, PEG, PAA, PEI, PMAO, and PMAO-PEG [24–28]. However, many of the existing polymer coatings face the challenge of chemical, thermal, and biological degradation, high shrinkage during curing, poor moisture resistance, and relatively poor mechanical properties. Epoxy resin is a complex polymer that has excellent moisture and chemical resistance, low shrinkage during curing, high impact resistance, and good mechanical and fatigue properties. However, the coefficient of friction (COF) of epoxy coatings is relatively high at 0.56–0.59 which hinders its application as a coating [29,30]. Its properties can, however, be improved with various additives [31,32].

Many oil and gas industries use metallic alloys for offshore oil drill, chemical plants, and hydrogen production from seawater. These alloys are subjected to highly corrosive environments of salt, water, and oxygen. The salt component of seawater accelerates the oxidation process and therefore increases the rate of corrosion [1]. Water and oxygen contents of the seawater and atmosphere permit the establishment of electrochemical corrosion [33,34]. To date, research efforts have been primarily concentrated on developing corrosion inhibition coatings capable of resisting both corrosion in saline environments and electrochemical corrosion [35,36]. Corrosion inhibitors are additives in coatings that diminish, delay, or even prohibit corrosion [37,38]. However, they may also induce a high level of toxicity and can be expensive [38,39]. Also, the same corrosion inhibitor may not be suitable for multiple alloys [40]. Metallic chromium has excellent anti-corrosion properties and is routinely used in steel as an anti-corrosive agent [41–44]. This is so because Cr metal forms a passivating oxide layer when in contact with oxygen. This passivating oxide layer film protects the metal underneath. In addition, being a transition metal, it has good hardness and thermal properties. Similarly, Ni forms a passivating oxide layer at room temperature which protects the metal underneath [44–47]. Traditionally, it has been used to plate brass and iron. As a transition metal, it also has good hardness and thermal properties.

Despite recent progress in advanced coatings, corrosion of metals and alloys in saltwater environments remain a big challenge. There are needs to produce coatings with corrosion resistance for saltwater environments, greater reliability, and ease of fabrication. Additionally, the market demands these coatings to be tunable for desired properties including strength, longevity, and desired friction, while maintaining a low cost. The objective of this research is to develop metal-ceramic composite coatings with satisfying frictional and corrosion performance while allowing for easy fabrication which competes with the epoxy coatings in published literature.

Materials and Methods

Preparation of Coating Formulations. Two coatings were developed and characterized in this research and are shown in Table 1. Three samples of each coating were used in each test to provide an average measurement.

Table 1 Compositions by weight percent of the two coatings developed in this research and particle sizes used

Value	D.E.R. 331 resin (%)	200 proof Ethyl alcohol (%)	Graphite (%)	SiC (%)	BN (%)	Cr (%)	Ni (%)
Coating 1	57.17	38.90	2.46	0.49	0.49	0.49	0
Coating 2	57.17	38.90	2.46	0.49	0.49	0	0.49

The resin (D.E.R. 331, *DOW Chemicals* (Midland, MI), density = 1.16 g/ml) to alcohol (C_2H_5OH, 200 proof, 100%, *VWR*, density = 0.789 g/ml) mixture was used to suspend the additives and allow for quick and easy coating application, with alcohol acting as a solvent to enable easier mixing of all ingredients. The specific ratio of resin-to-alcohol was chosen so the alcohol would dissolve all resin with no excess alcohol and was discovered by rigorous trials. Graphite acted as a friction modifier, while SiC (*Sigma-Aldrich* (St. Louis, MO), 400 mesh, density = 3.22 g/ml) and BN (*Sigma-Aldrich*, <1 μm, 98% pure, density = 2.29 g/ml) worked to both modify friction and enhance wear performance. Cr (*Sigma-Aldrich*, 325 mesh, 99% pure, density = 7.14 g/ml) and Ni (*Sigma-Aldrich*, <50 μm, 99.7% pure, density = 8.91 g/ml) were added in their respective coatings to inhibit corrosion. To fabricate the coatings, the general procedure was followed. First, respective amounts of resin and ethyl alcohol were added and mixed until fully blended and homogeneous. Next, respective amounts of additive powders were then fully blended separately. This was done to ensure complete mixing of all powders and so no agglomerations would occur. Last, powder mixture was added to resin/alcohol mixture and stirred until a full blend was attained. Results were compared with 1010 carbon steel (1/4 hard temper) substrates (composition shown in Table 2). Substrate dimensions were 1.27 cm × 1.27 cm × 0.51 cm.

After the fabrication of the coating mixtures, substrates were cleaned first using acetone then followed by ultrasonic cleaning to remove any rust and foreign materials from the substrate surface. Samples were finally air-dried so no moisture was left to mix with the coating. A thin layer of the respective coatings was then applied to the cleaned substrates' top surfaces by brush and subsequently set at room temperature for 1 hour. The brush method is common when applying epoxy coatings prior to curing, as the curing process generally results in a uniformed surface [48]. The coating material was in quasi-liquid form when applied by brush. Thus, due to gravitational forces in combination with the removal of the excess ethanol when the sample was in the oven, the surface of the coating solidified to form a smooth coating. This was to ensure the coating on each sample did not form any precipitates or agglomerations and fully covered the sample's surface. The samples were then placed in an electric furnace at 200 °C for 48 h to fully cure, under the flashpoint of 252 °C of the resin. The resultant coatings had an average thickness of 0.23 mm with a standard deviation of 0.079 mm.

Characterization and Testing. Corrosion resistance was tested for both coatings using salt spray (SS) corrosion and electrochemical corrosion. The results were compared with the substrates. For salt spray corrosion, samples were first ultrasonically cleaned to remove any deposits on the surface. This was followed by air drying. After that, the samples were weighed and the weights were recorded. The samples were then placed in *a WTP 160 Premium Salt Spray Chamber* (*Inland Testing Equipment*) for 48 h. To accelerate corrosion in a saline environment, the chamber was set at 45 °C under atmospheric pressure. A solution of 5 wt% solution of NaCl in DI water was used as the corrosive agent. As noted, the salt spray is an accelerated test commonly used in industry [49–51]. The elevated temperature with salt fog enabled short duration examination of long-term corrosion resistivity. As such, the test was designed for a duration of 48 h. The corrosion was visible. After the samples underwent vigorous corrosion conditions for 48 h, they were then taken out of the chamber, ultrasonically cleaned, air-dried, and weighed again. These measured weights were compared with their initial weights. The weight measurements had an accuracy of ±0.0001 g. This environment and time resulted in the visual development of pitting and rust on the carbon steel samples.

For electrochemical testing, potentiodynamic polarization experiments were performed using *Gamry Reference 600* hardware in parallel with *Gamry Framework* and *Gamry Echem Analyst*

Table 2 Composition by weight percent of the substrate

Element	C	Mn	P	S	Si	Ni	Cr	Mo	Al	Cu	Fe
%	0.09	0.38	0.009	0.01	0.012	0.03	0.046	0.01	0.039	0.038	99.336

software. To prepare samples, they were first sealed in liquid electrical tape on all sides except the top surface, giving each sample an exposed surface area of 1.6129 cm^2 during testing. Tests were performed in a 3.5 wt% solution of NaCl in DI water with the sample as the working electrode, an Ag (s)/AgCl(aq.) reference electrode, and a graphite counter electrode. The voltage potential ranged from −1.5 V to + 1.5 V versus open circuit potential (E_{oc}). During these tests, the scan rate was 10 mV/s, the sample period was 0.1 s, and the initial delay was 100 s or stability of <0.05 mV/s, whichever occurred first. The resultant potentiodynamic polarization curves were used to quantify the corrosion performance of the coatings in contrast to that of the substrate.

Coefficient of friction experiments were performed on both coatings. For these tests, a *CSM Instruments* tribometer was used. The counterpart was a 6 mm diameter E52100 bearing steel ball which slid in a linear reciprocating motion. There were 325 cycles per test with a maximum speed of 4 cm/s, a track length of 6 mm, an applied load of 3 N, and an acquisition rate of 20 Hz. Scratch tests were also performed using the same tribometer using a tungsten carbide tip. For this, unidirectional scratches were made with a maximum speed of 0.1 cm/s, a track length of 6 mm, a maximum speed of 0.1 cm/s, a load of 1 N, and a test duration of 25 s. Two scratch tests were performed on each sample: one where the scratcher tip was let down hard and thus punctured the surface of the coatings, and one where the scratcher tip was let down gently and did not puncture the coating.

Knoop hardness tests were run on each coating and substrate for comparison. Tests were performed using a *LECO DM-400 LF* microhardness tester. For each test, a load of 300 gf and a test time of 15 s was used. Five tests were run on each coating and substrate, and their averages and standard deviations were calculated. From these tests, the average substrate hardness was 218.6 with a standard deviation of 17.1, the average hardness of coating 1 was 24.5 with a standard deviation of 5.8, and the average hardness of coating 2 was 27.9 with a standard deviation of 2.5. The coating hardness values are similar to those of PET, urethane, and polyester coatings [52,53].

To study the morphological effects of corrosion on the coatings, optical microscopy and interferometry were utilized. Magnification with optical microscopy ranged from 50 × to 200 ×. Pits, corrosion products, and overall morphology were visualized for the coatings and substrates. Interferometry was used to measure surface roughness before and after corrosion for the coatings and substrates.

Results and Discussion

Accelerated Corrosion Evaluation in Salt Fog. Salt spray corrosion tests were performed to assess the performance of the coatings in harsh and corrosive environments. Table 3 displays the average weight loss of the two coatings and substrate after 48 h in the salt spray chamber. Three samples of each type were measured. Samples were all placed evenly spaced and equally distanced from the salt spray nozzle. When compared with the initial weights (second row), the substrates lost an average of 1.4%, coating 1 lost an average of 0.06%, and coating 2 lost an average of 0.01% of its initial weight (fifth row). As seen from the fourth row, compared with the substrate weight loss (0.0233 g), coating 1 lost about 4.3% (0.001 g) as much mass as the substrate, while coating 2 lost about 0.9% (0.0002 g). Hence, the coated samples lost a minuscule percentage of weight loss of the substrate. Thus, Table 3 clearly shows the effectiveness of the coatings to prevent corrosion in saline environments.

Table 3 Average weight loss after 48 h for the substrate and two coatings

Measured quantity	Substrate	Coating 1	Coating 2
Initial weight (g)	1.6700	1.7400	1.7600
Weight after corrosion test (g)	1.6467	1.7390	1.7598
Weight loss (g)	0.0233	0.0010	0.0002
% Weight loss based on initial weight	1.3952	0.0575	0.0114
% Weight loss based on substrate weight loss	100	4.29	0.86

Electrochemical Performance. Figure 1 shows potentiodynamic polarization curves for the substrate and coatings. In this figure, the *y*-axis is the controlled potential versus the Ag/AgCl reference electrode potential, and the *x*-axis is the measured current density. Potential describes the thermodynamics taking place in the reaction while current density describes kinetics. The horizontal section of each curve marks the corrosion potential E_{corr} and corresponding corrosion current density i_{corr}, which can be calculated by fitting lines to the portions just above and below this horizontal point (Tafel region). The values of E_{corr} and i_{corr} were calculated using the Tafel extrapolation method [54], and the results are shown in Table 4. A higher E_{corr} indicates more nobility of the working electrode and thus less likelihood to corrode while a lower E_{corr} indicates more activity and more likelihood to corrode. Likewise, a curve further to the left generally implies a slower reaction and lower corrosion rate since i_{corr} will be lower, while a curve further to the right implies a faster reaction and higher corrosion rate. As such, the curves for both coatings are to the left of the substrate showing their decreased corrosion rates.

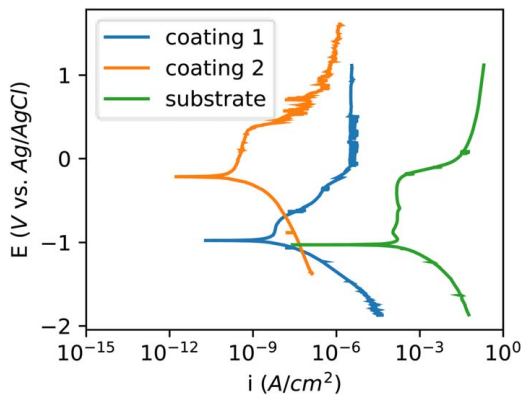

Fig. 1 Potentiodynamic polarization curves for the substrate and two coatings

Table 4 Average values of i_{corr} and E_{corr} for the coatings and substrate

Value	Substrate	Coating 1	Coating 2
i_{corr} (A/cm^2)	1.16×10^{-3}	4.40×10^{-9}	2.73×10^{-10}
E_{corr} (V versus E_{ref})	−1.00	−0.50	−0.04

The Tafel region of coating 2 is further to the left and higher than that of coating 1, meaning coating 2 has improved corrosion performance over coating 1. Additionally, the horizontal spikes in the vertical portion above the Tafel region of the potentiodynamic curves (passive region) and topmost portion (transpassive region) indicate that pitting occurred in all samples.

Each coating and substrate were tested at least three times and their corrosion current densities (i_{corr}) and corrosion potentials (E_{corr}) were measured using Gamry software. The average values for i_{corr} and E_{corr} for each surface are displayed in Table 4. This table shows similar trends to the weight loss data from salt spray testing. The substrate had the highest i_{corr} and lowest E_{corr}, indicating that it is the least resistant to corrosion. Coating 2 meanwhile had the lowest i_{corr} and highest E_{corr}, indicating that it is the most resistant. The coatings' i_{corr} values were about a factor of 10^7–10^8 less than that of the substrate, showing their superior performance. In addition, the passive region of coating 2 exists over a larger potential range than that of coating 1, showing coating 2 has a more stable passive region.

It has been widely accepted that nickel is nobler than chromium. The reduction potential for Ni is −0.25 eV (gaining 2 e^-) and Cr −0.744 (3 e^-). Because of this, the coating 2 that consists 49 wt% Ni is more corrosion resistant than coating 1 that has the same amount Cr wt%. The design consideration, theory, and experimental data agree with each accordingly.

Surface Integrity. Coated samples and substrate were examined before corrosion (BC), after salt spray corrosion, and after electrochemical corrosion using optical microscopy. This was done to observe the differences in their surfaces due to corrosion. All samples were ultrasonically cleaned prior to examination to remove any unwanted salt deposits. Figures 2(*a*)–2(*i*) show the corresponding images for the substrate, coating 1, and coating 2, respectively. All images shown were taken at 100× magnification. In Figs. 2(*a*)–2(*c*), corrosion products and pitting appear after salt spray corrosion and electrochemical corrosion, with electrochemical corrosion exhibiting the most corrosion products and most severe pitting. The corrosion products and pitting are labeled in Fig. 2(*b*) for reference. There were eight distinguishable pits after salt spray corrosion and more than 60 pits after electrochemical corrosion. In contrast, there is very little change between the surface before corrosion, after salt spray corrosion, and after electrochemical corrosion in the coated samples as seen in Figs. 2(*d*)–2(*f*) for coating 1 and Figs. 2(*g*)–2(*i*) for coating 2. Instead, there is almost no distinguishable difference between the images, showing the coatings' effectiveness at preventing corrosion. Additionally, the morphologies of the coatings appear much more uniform than that of the substrate. Almost no visible pits formed across any of the coatings after salt spray corrosion and no corrosion products were visible. Only a small amount of corrosion products and a few pits were visible after electrochemical corrosion on the coatings. As such, there is little to differentiate between the two coatings.

Frictional Performance. The friction performance of the coatings was tested and compared. It is important to note that the counterpart exhibited no damage during these tests. Figure 3(*a*) shows the results of the COF test performed on coating 1. In this figure, the *y*-axis is COF and frictional force, and the *x*-axis is time and laps. Over a period of 325 laps, the coating maintains its low COF of approximately 0.1. This shows the stability of the coating during friction testing, indicating its long-lasting performance and low friction. Low COF is due to the friction-reducing effects of the additives in the epoxy resin matrix.

Friction performance for coating 2 is shown in Fig. 3(*b*). The COF is 0.1 to begin with and then reaches a steady-state value of about 0.17. The COF is approximately 38% the value of a blank substrate steel-on-steel contact (COF = 0.45) [55]. However, coating 2 has a slightly higher COF compared with coating 1. This is attributed to the presence of Ni in coating 2. Compared with Cr (in coating 1), the presence of Ni in coating 2 imparts it a better corrosion property (Fig. 1). However, it also simultaneously affects its frictional performance. Nevertheless, the introduction of

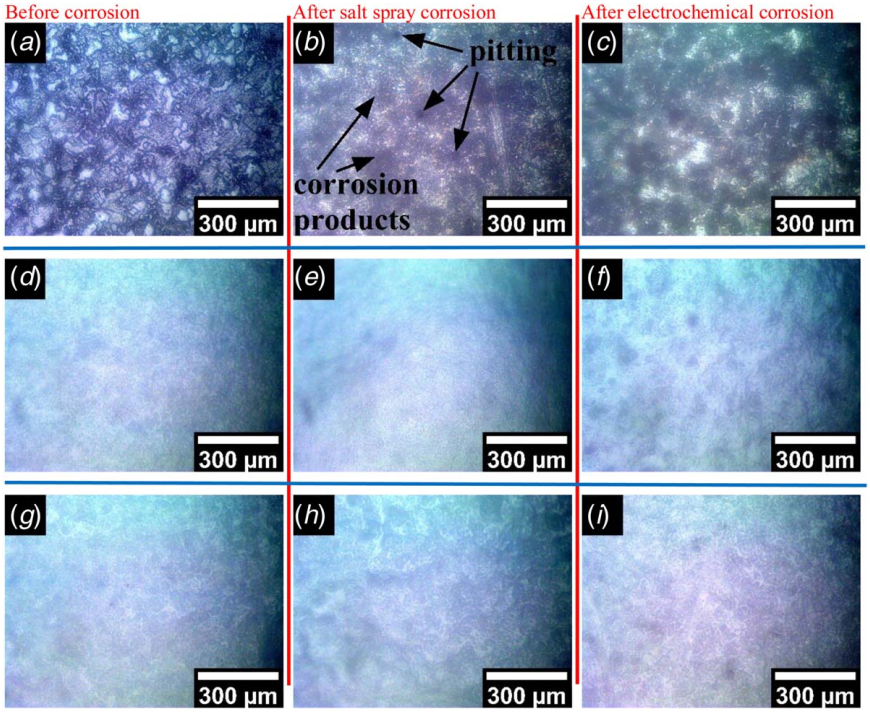

Fig. 2 Optical microscopic images of the substrate (first row), coating 1 (second row), and coating 2 (third row); before corrosion (first column), after salt spray corrosion (second column), and after electrochemical corrosion (third column). 100× magnification was used.

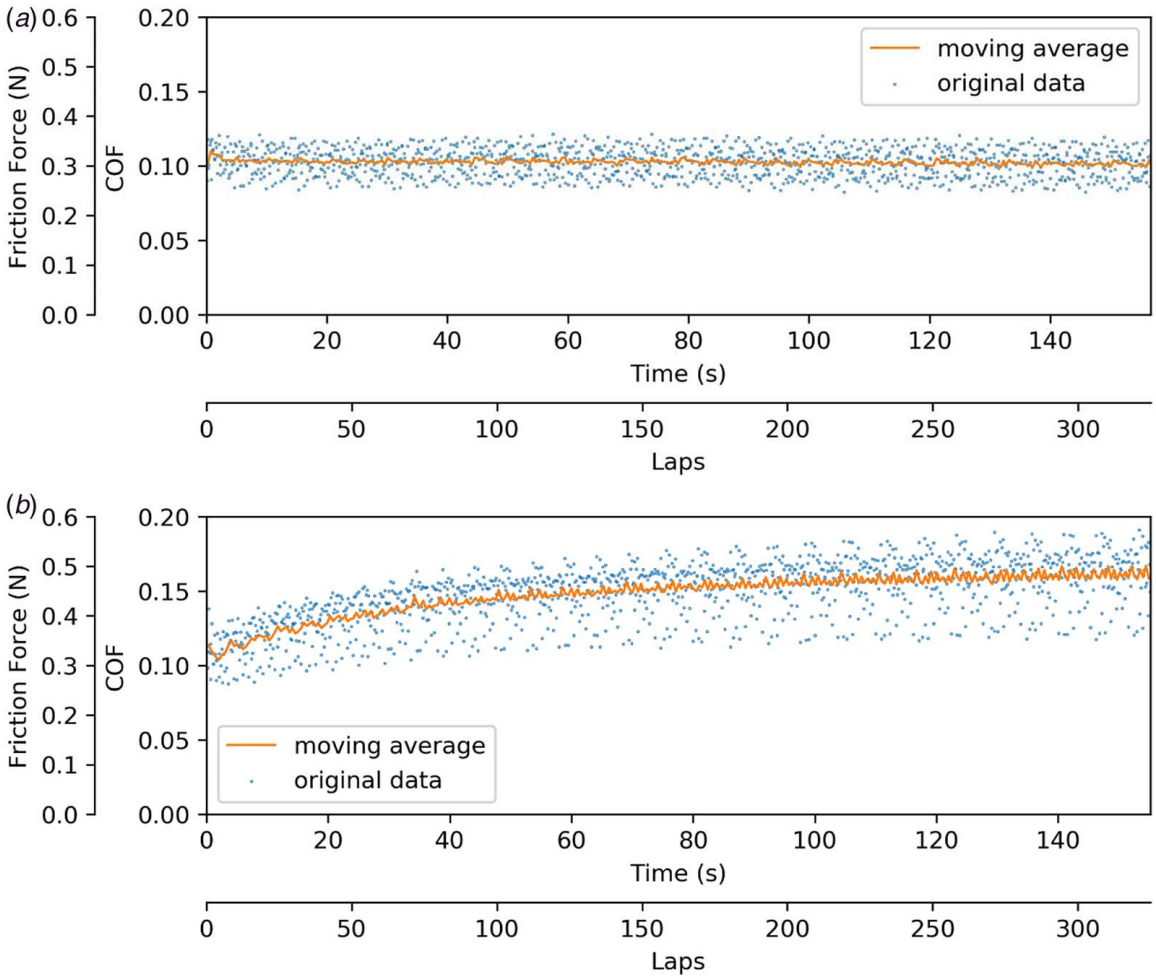

Fig. 3 (*a*) COF test results for coating 1 and (*b*) COF test results for coating 2

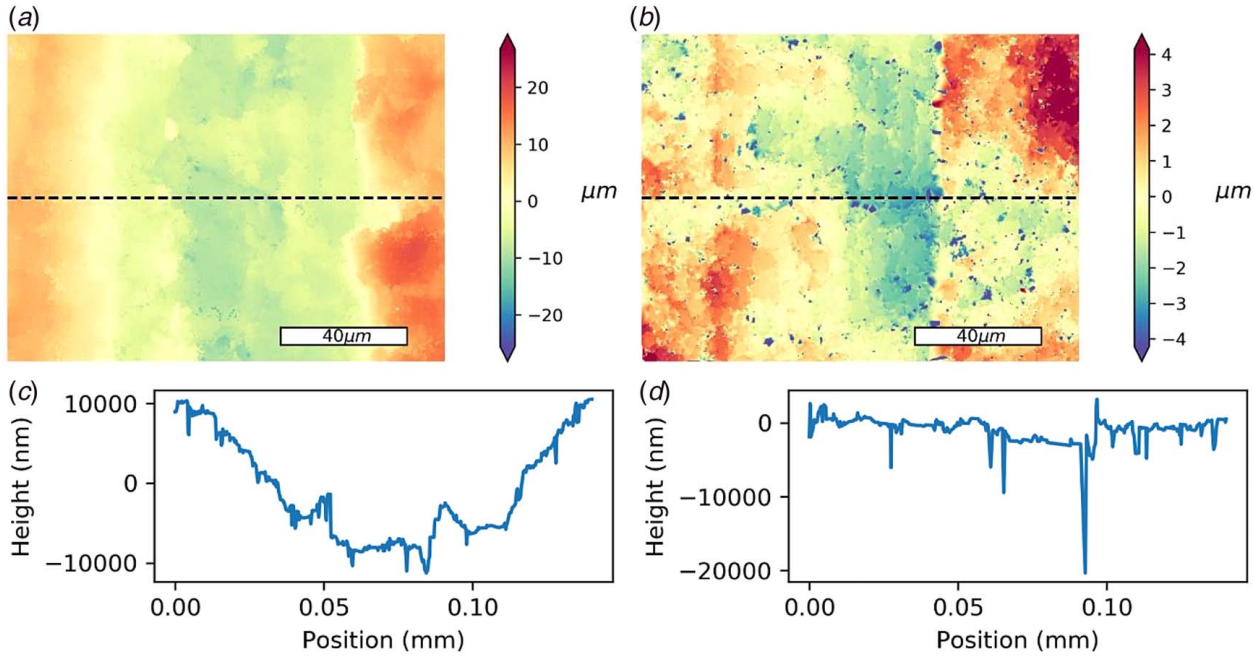

Fig. 4 Interferometer images and profiles of scratch tests on sample coating 1. The left two images show a deep scratch, and the right two images show a shallow scratch.

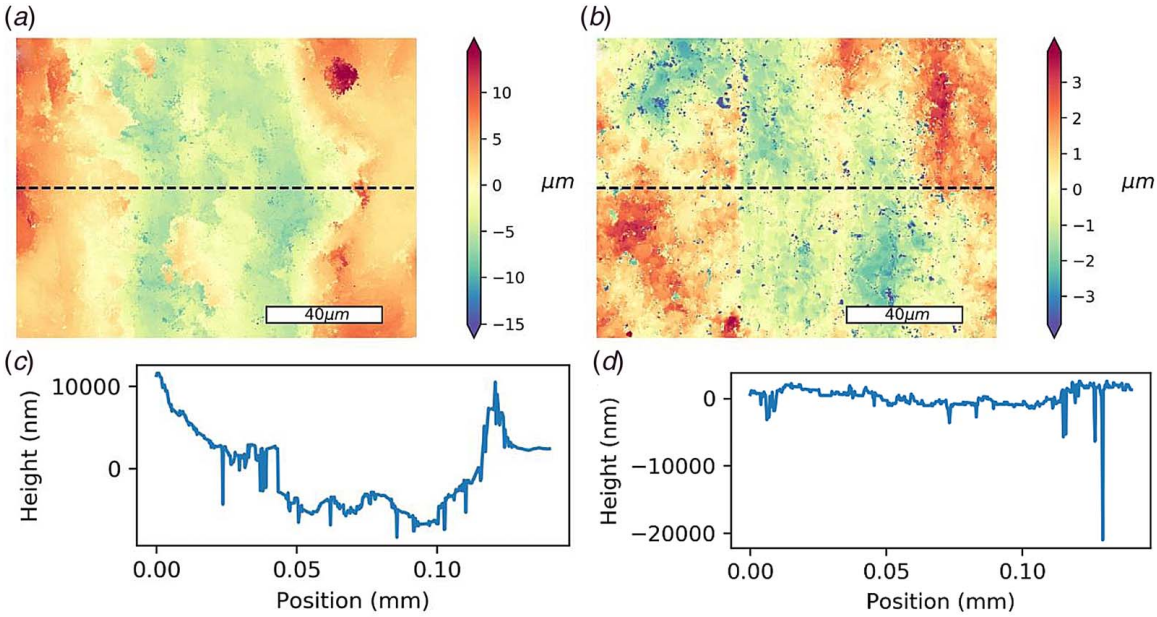

Fig. 5 Interferometer images and profiles of scratch tests on sample coating 2. The left two images show a deep scratch, and the right two images show a shallow scratch.

Ni in coating 2 is overall advantageous for both its corrosion and frictional performance.

Scratch Resistance. Scratch tests were performed on the coatings to understand the wear behavior. The scratch tests on the coatings exhibited unique scratch performances. Figures 4 and 5 show the interferometer images and cross-sectional profiles for coating 1 and coating 2, respectively. Two scratch tests were performed on each sample: one where the scratcher tip was let down hard and thus punctured the surface of the coatings (for coating 1: Figs. 4(*a*)–4(*c*); for coating 2: Figs. 5(*a*)–5(*c*)), and one where the scratcher tip was let down gently and did not puncture the coating (for coating 1: Figs. 4(*b*)–4(*d*); for coating 2: Figs. 5(*b*)–5(*d*)). These resulted in two very different scratch profiles as seen. The scratch profile for coating 1 where the tip was let down hard resulted in scratches ~ 20 μm deep, with a slightly shallower scratch for coating 2 (~16 μm deep). However, the scratch profile for coating 1 where the tip was let down gently resulted in a slight scratch (~4 μm deep), and for coating 2 the scratch was hard to distinguish from the rest of the coating even with interferometry. Thus, the scratch tests showed little to no wear of the coatings. This is due to the presence of ceramics SiC and BN which impart the coatings' unique hardness characteristics. Also, it is seen that the presence of Ni (in coating 2) tends to improve the scratch and thus wear resistance of the coating formulation. The scratch profiles here show that the coatings experience low wear from the scratch test due to the combination of the high-hardness of additives and low COF. However, once a wear track piercing the coating is initiated, the material is removed more easily due to the low wear resistance of the epoxy matrix.

Roughness. Interferometry was used to measure the roughness of each coating and substrate. Roughness was measured at least three times each before corrosion, after salt spray corrosion, and after electrochemical corrosion. Both arithmetic average roughness (Ra) and root mean square roughness (RMS) were measured and the measurements were averaged (Table 5). RMS and Ra are among those commonly used parameters in industry [56–58]. Using these two parameters assisted the authors to not only evaluate the minimal changes on the surface profile, but also the accuracy of the measurement. As such, both RMS and Ra were chosen to describe variation in surface roughness in this research in order to confirm the effect of corrosion on surface roughness.

From these measurements (Fig. 6(*a*)), BC, the substrate had the lowest average roughness (1.06 μm), followed by coating 1 (1.31 μm), and then coating 2 (1.74 μm). After salt spray corrosion (Fig. 6(*b*)), the average substrate roughness (Ra) does not change, while the root mean squared roughness RMS increases slightly from 1.26 μm to 1.34 μm. Both Ra and RMS for the coatings increase (Fig. 6(*b*)). Considering the uncorroded substrate had many scratches, the corrosion products of the substrate after the SS corrosion seemed to have filled the surface troughs resulting in a negligible increase in surface roughness. The highly corrosive salt chamber environment induces pit formation on coated surfaces leading to somewhat higher surface roughness. A higher Ra and RMS for coating 2 compared with that of coating 1, in both SS (Fig. 6(*b*)) and after EC (Fig. 6(*c*)) suggests that the presence of Cr in coating 1 imparts more pitting resistance to the coating compared with the presence of Ni in coating 2. This is because Cr is more reactive than Ni in the electrochemical series. Hence, the presence of Cr leads to slightly higher corrosion products (in coating 1) which get deposited in the surface troughs leading to more balancing out of the Ra or RMS.

For better comparison, the Ra (Fig. 6(*d*)) and RMS (Fig. 6(*e*)) are plotted for each treatment. The Ra and RMS values for treatment SS followed the order S < C1 < C2 while that for treatment EC followed the order C1 < S < C2. Thus, the two coatings and substrate show

Table 5 Average roughness of substrate (S), coating 1 (C1), and coating 2 (C2) BC, after SS corrosion, and after EC

Value	S-BC	S-SS	S-EC	C1-BC	C1-SS	C1-EC	C2-BC	C2-SS	C2-EC
Ra (μ)	1.055	1.056	2.676	1.311	2.131	1.494	1.740	2.554	3.107
RMS (μ)	1.263	1.34	3.731	1.855	2.752	1.999	2.419	3.063	3.873

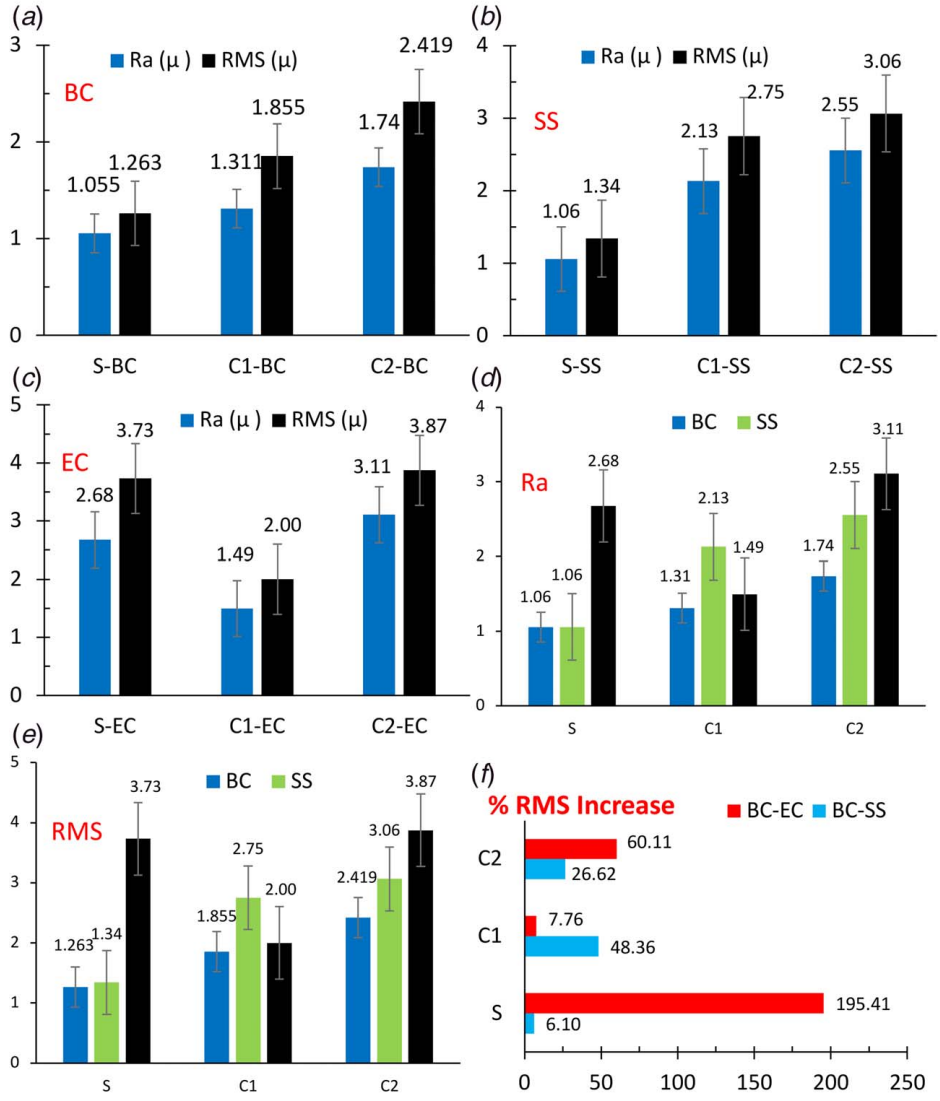

Fig. 6 Average roughness (Ra) and RMS roughness of substrate (*S*), coating 1 (C1), and coating 2 (C2): (*a*) BC, (*b*) after SS corrosion, (*c*) after EC, (*d*) Ra variation, (e) RMS variation, and (*f*) % RMS increase between treatments BC to SS (BC-SS) and BC to EC (BC-EC)

different corrosion behaviors in saltwater (at high temperature) and electrolyte solution. To better understand these effects, the percentage increase in RMS roughness based on BC values has been plotted in Fig. 6(*f*) for increase between treatments BC to SS (BC-SS) and BC to EC (BC-EC). The percentage increase in RMS roughness is the highest for the substrate for BC-EC followed by coating 2 and then coating 1. This suggests that the substrate surface is most affected due to the electrochemical corrosion compared with that of the coatings. Additionally, coating 1 is most resistant to pitting corrosion in EC conditions due to the presence of Cr. In the BC-SS comparison, coating 2 has a smaller % RMS increase compared with coating 1. Thus, in saltwater and at high temperatures, coating 2 is relatively more effective than coating 1 in terms of resistance to pit formation. The substrate has the least pit formation in

Table 6 Comparison between the coatings in this research and state-of-the-art

Material	COF	i_{corr} (A/cm^2)	E_{corr} (V versus Ag/AgCl)	Reference
Coating 1	0.1	4.40×10^{-9}	−0.5	This work
Coating 2	0.17	2.73×10^{-10}	−0.04	This work
Epoxy	0.56–0.59	3.07×10^{-9}–8.09×10^{-6}		[29,30,59]
Graphite + epoxy	0.32–0.38			[29]
Carbon modified Celatom + epoxy	0.27	1.75×10^{-9}		[30]
Oily Celatom + epoxy	0.16	3.28×10^{-11}		[30]
FG + epoxy	0.6–0.65	1.29×10^{-6}–2.84×10^{-6}	−0.505–−0.466	[59]
FC60 + epoxy	0.6–0.65	2.07×10^{-6}–3.73×10^{-6}	−0.565–−0.540	[59]
PTFE + epoxy	0.13–0.66			[60]
Ti_3C_2 + epoxy	0.17–0.24	3.39×10^{-8}–7.05×10^{-7}	−0.486–−0.246	[61,62]
PEEK	0.2–0.4			[63,64]

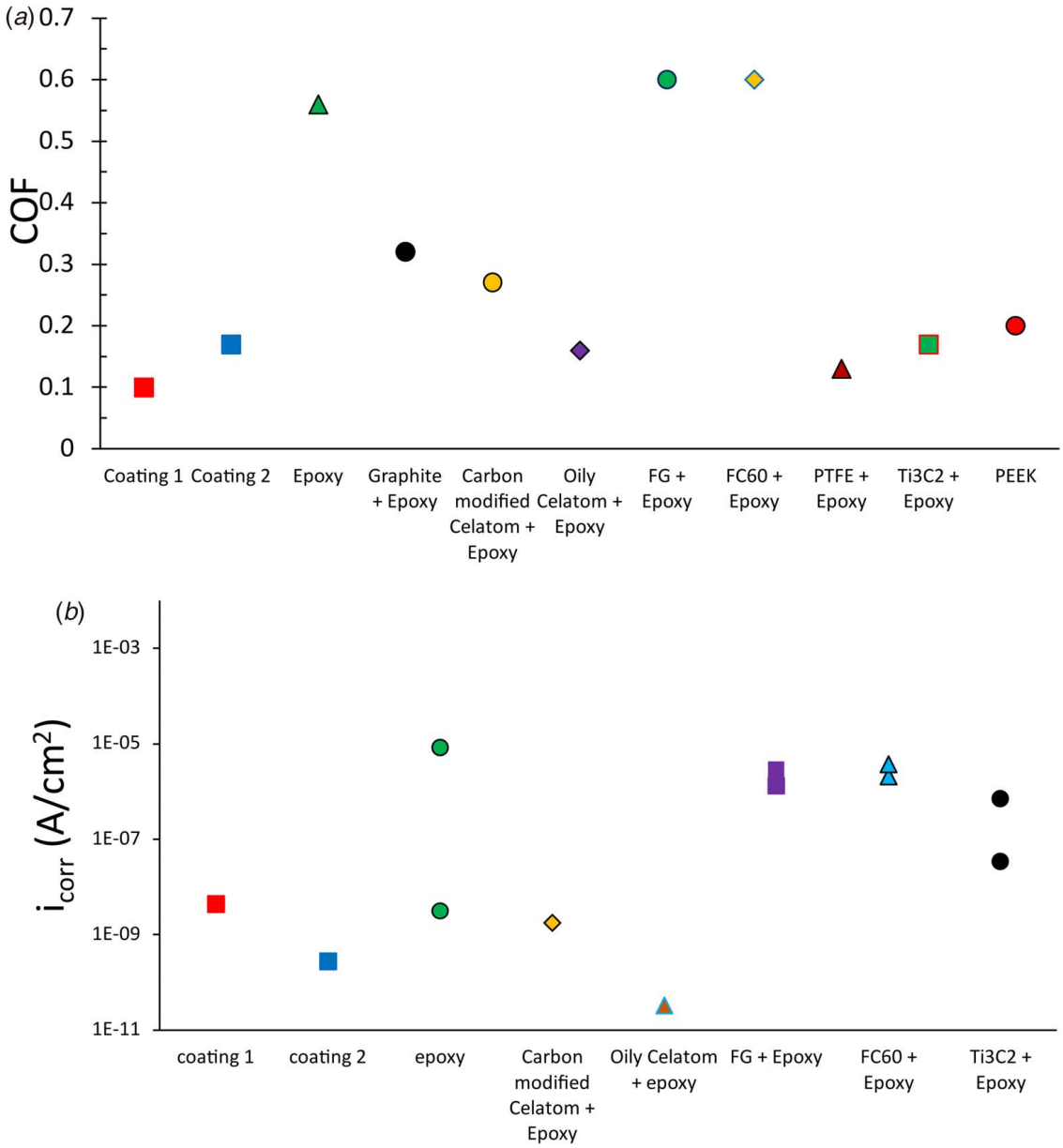

Fig. 7 (*a*) COF and (*b*) i_{corr} literature values from Table 6 plotted with the values of the two coatings studied in this research

BC-SS. It is to be noted that merely Ra and RMS data is not sufficient in evaluating coating resistance to corrosion. Instead, the overall effects of i_{corr}, E_{corr}, hardness, scratch resistance, and microstructure need to be assessed simultaneously when analyzing coating performance. Hence, considering all these assessments, the coated samples impart higher corrosion protection to the substrate.

Comparison With State-of-the-Art Coatings. Table 6 displays published literature on some state-of-the-art coatings and presents a comparison with the coatings synthesized in this work.

Of all these coatings, coating 1 developed in this research had the lowest COF (0.1) (second column in Table 6) and one of the lowest corrosion current densities i_{corr} (4.40×10^{-9} A/cm^2) (third column in Table 6). Coating 2 had one of the lowest COF (0.17) and the second lowest corrosion current density (2.73×10^{-10} A/cm^2). The only coating lower was that of oily Celatom + epoxy. Both coatings outperformed common coatings such as PEEK and PTFE in epoxy. Thus, this coating has extremely high performance. Additionally, the coatings in this research clearly performed far better than epoxy on its own, and the COF of these coatings performed far better than graphite in epoxy as well. To obtain a better visual comparison, Fig. 7 was obtained which shows the performance of the coatings in this research against those in literature. Note that for Fig. 7(*a*), the lowest measured COF value was plotted for each type of coating, and for Fig. 7(*b*), the highest and the lowest i_{corr} value was plotted for coatings with multiple published values. The coatings in this research (shown with the square farthest to the left (coating 1) and square second farthest to the left (coating 2)) greatly decreased the COF relative to literature values of epoxy resin (Fig. 7(*a*)). The maximum COF reduction was up to six times lower by coating 1 and up to three times lower by coating 2. The corrosion current density of coating 2 was lower than all epoxy values (up to five orders of magnitude lower than some reports), and the corrosion current density of coating 1 was lower (up to three orders of magnitude lower than some reports) than all but one literature value (Fig. 7(*b*)). Thus, this coating clearly both prevents corrosion and reduces COF due to the composition of the coating. A schematic of this is shown in Fig. 8. It has been reported that the use of epoxy as coatings to protect metals and

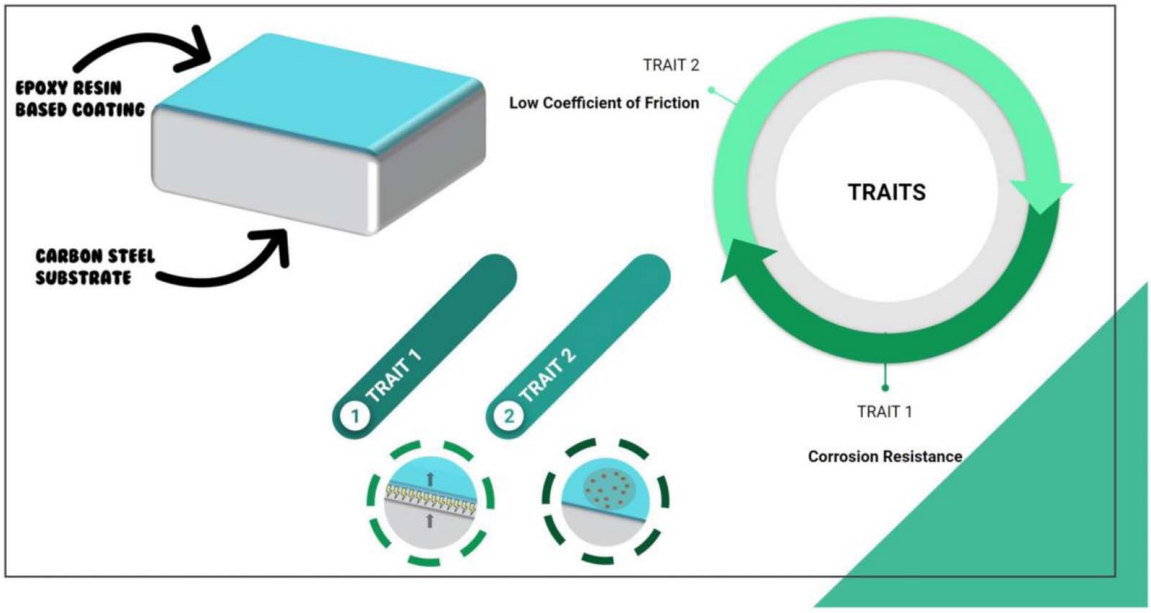

Fig. 8 A schematic of the coating, underlining its attractive COF and corrosion performance

alloys [65–69]. Those coatings have been widely used on carbon steel pipelines in the oil and gas industry [70] and heat exchangers [71]. Additives in the coatings can improve the durability of epoxy coatings to wear [72,73], which is beneficial due to the low COF seen in the coatings in this research. As such, the vast improvement in terms of corrosion rate and COF in this work over that of epoxy coatings indicates the attractiveness of these coatings in various applications.

Conclusion

In this research, metal-ceramic composite coatings bonded with epoxy were developed which showed promising corrosion resistance. These coatings were low cost and easy to fabricate, making them attractive for applications where corrosion resistance and frictional performance is required. The maximum COF reduction was six times lower in the coatings, i.e., 0.10 for coatings with Cr and 0.17 for coatings with Ni, compared with a COF 0.56–0.59 for epoxy. Corrosion current density in coatings with Ni in this research measured by potentiodynamic polarization testing was about five orders of magnitude lower than epoxy coatings reported in literature. Mass loss due to salt spray corrosion testing in coatings with Ni was 1/100 that of the carbon steel substrate. Additionally, little to no corrosion deposits were visible on all coatings under optical microscopy, while the substrate had a large amount of corrosion deposits. This shows that these coatings are extremely useful in marine application, where corrosion protection from seawater is essential. For the electrochemical corrosion tests, the i_{corr} values were 1.16×10^{-3} A/cm^2, 4.40×10^{-9} A/cm^2, and 2.73×10^{-10} A/cm^2 for the substrate, the coating with Cr as an additive, and the coating with Ni as an additive, respectively. This indicates that corrosion was lower in those two coatings by six to seven orders of magnitude relative to the substrate. The coatings showed exceptional corrosion resistance compared with that of the carbon steel substrate. The coefficient of friction of the coating with Cr as an additive was 0.1 and that of the coating with Ni as an additive was 0.17. Both coatings outperformed a variety of epoxy-based coatings published in literature in terms of frictional performance. These coatings also showed desirable friction performance. Due to high corrosion resistance, considerable friction performance, ease of synthesis, and low cost, these coatings provide excellent alternatives in a variety of industrial applications.

Funding Data

Part of this research was supported by NPRP grant (NPRP10-0101-170081) from the Qatar National Research Fund (a member of Qatar Foundation). Peter Renner was supported by the National Science Foundation (NSF) Graduate Research Fellowship.

Conflict of Interest

There are no conflicts of interest.

References

[1] Revie, R. W., 2008, *Corrosion and Corrosion Control: An Introduction to Corrosion Science and Engineering*, John Wiley & Sons, New York.
[2] Shreir, L. L., 2013, *Corrosion: Corrosion Control*, Newnes, London.
[3] Kutz, M., 2018, *Handbook of Environmental Degradation of Materials*, William Andrew, London.
[4] Paul, S., 2012, "Modeling to Study the Effect of Environmental Parameters on Corrosion of Mild Steel in Seawater Using Neural Network," ISRN Metall., **2012**, pp. 1–6.
[5] Zhang, J., and Li, N., 2007, "Analysis on Liquid Metal Corrosion–Oxidation Interactions," Corros. Sci., **49**(11), pp. 4154–4184.
[6] Selvam, K., Saini, J., Perumal, G., Ayyagari, A., Salloom, R., Mondal, R., Mukherjee, S., Grewal, H. S., and Arora, H. S., 2019, "Exceptional Cavitation Erosion-Corrosion Behavior of Dual-Phase Bimodal Structure in Austenitic Stainless Steel," Tribol. Int., **134**, pp. 77–86.
[7] Mokhatab, S., Poe, W. A., and Mak, J. Y., 2018, *Handbook of Natural Gas Transmission and Processing: Principles and Practices*, Gulf Professional Publishing.
[8] Renner, P., Jha, S., Chen, Y., Raut, A., Mehta, S. G., and Liang, H., 2021, "A Review on Corrosion and Wear of Additively Manufactured Alloys," ASME J. Tribol., **143**(5), p. 050802.
[9] Lee, K., Dai, W., Naugle, D., and Liang, H., 2018, "Effects of Microstructure of Quasicrystal Alloys on Their Mechanical and Tribological Performance," ASME J. Tribol., **140**(5), p. 051605.
[10] Dai, W., Lee, K., Sinyukov, A. M., and Liang, H., 2017, "Effects of Vanadium Oxide Nanoparticles on Friction and Wear Reduction," ASME J. Tribol., **139**(6), p. 061607.
[11] Choi, H., Lee, K., Reeks, J., and Liang, H., 2016, "Design and Synthesis of a Superhydrophobic PVDF-Based Composite," ASME J. Tribol., **138**(2), p. 022301.
[12] Shin, Y., Xiao, H., and Liang, H., 2015, "A Novel Composite With Nacreous Reinforcement for Corrosion and Wear Reduction," ASME J. Tribol., **137**(2), p. 021602.
[13] Barkley, B., Sanchez, C., and Liang, H., 2012, "In Situ Strengthening of the Aluminum-Based Gadolinium Alloy Composite for Tribological Applications," ASME J. Tribol., **134**(1), p. 011603.
[14] Huitink, D., Zarrin, T., Sanders, M., Kundu, S., and Liang, H., 2011, "Effects of Particle-Induced Crystallization on Tribological Behavior of Polymer Nanocomposites," ASME J. Tribol., **133**(2), p. 021603.

[15] Fox, G. R., and Liang, H., 2010, "Wear Mode Comparison of High-Performance Inconel Alloys," ASME J. Tribol., **132**(2), p. 021603.
[16] He, X., Chiu, C., Esmacher, M. J., and Liang, H., 2013, "Nanostructured Photocatalytic Coatings for Corrosion Protection and Surface Repair," Surf. Coat. Technol., **237**, pp. 320–327.
[17] Fevzi Ozaydin, M., and Liang, H., 2016, "Design and Synthesis of a Geopolymer-Enhanced Quasi-Crystalline Composite for Resisting Wear and Corrosion," ASME J. Tribol., **138**(2), p. 021601.
[18] Daroonparvar, M., Yajid, M. A. M., Bakhsheshi-Rad, H. R., Kumar, P., Kay, C. M., and Kalvala, P. R., 2020, "Fabrication and Corrosion Resistance Evaluation of Novel Epoxy/Oxide Layer (MgO) Coating on Mg Alloy," Prot. Met. Phys. Chem. Surf., **56**(5), pp. 1039–1050.
[19] Yuan, H., Qi, F., Zhao, N., Wan, P., Zhang, B., Xiong, H., Liao, B., and Ouyang, X., 2020, "Graphene Oxide Decorated With Titanium Nanoparticles to Reinforce the Anti-Corrosion Performance of Epoxy Coating," Coatings, **10**(2), p. 129.
[20] Chen, Y., Ren, B., Gao, S., and Cao, R., 2020, "The Sandwich-Like Structures of Polydopamine and 8-Hydroxyquinoline Coated Graphene Oxide for Excellent Corrosion Resistance of Epoxy Coatings," J. Colloid Interface Sci., **565**, pp. 436–448.
[21] Wu, Y., He, Y., Zhou, T., Chen, C., Zhong, F., Xia, Y., Xie, P., and Zhang, C., 2020, "Synergistic Functionalization of H-BN by Mechanical Exfoliation and PEI Chemical Modification for Enhancing the Corrosion Resistance of Waterborne Epoxy Coating," Prog. Org. Coat., **142**, p. 105541.
[22] Toorani, M., Aliofkhazraei, M., Mahdavian, M., and Naderi, R., 2020, "Effective PEO/Silane Pretreatment of Epoxy Coating Applied on AZ31B Mg Alloy for Corrosion Protection," Corros. Sci., **169**, p. 108608.
[23] Li, P., He, X., Huang, T.-C., White, K. L., Zhang, X., Liang, H., Nishimura, R., and Sue, H.-J., 2015, "Highly Effective Anti-Corrosion Epoxy Spray Coatings Containing Self-Assembled Clay in Smectic Order," J. Mater. Chem. A, **3**(6), pp. 2669–2676.
[24] Rohwerder, M., Isik-Uppenkamp, S., and Amarnath, C. A., 2011, "Application of the Kelvin Probe Method for Screening the Interfacial Reactivity of Conducting Polymer Based Coatings for Corrosion Protection," Electrochim. Acta, **56**(4), pp. 1889–1893.
[25] Gonzalez-Pech, N., and Grassian, V., 2018, *Surface Chemical Functionalities of Environmental Nanomaterials.*, Elsevier, San Diego, CA.
[26] Włoch, M., and Datta, J., 2020, "Rheology of Polymer Blends," *Rheology of Polymer Blends and Nanocomposites*, Elsevier, New York, pp. 19–29.
[27] Asmatulu, R., Nguyen, P., and Asmatulu, E., 2013, "Nanotechnology Safety in the Automotive Industry," *Nanotechnology Safety*, Elsevier, New York, pp. 57–72.
[28] Driver, M., 2012, *Coatings for Biomedical Applications*, Elsevier, New York.
[29] Pan, G., Guo, Q., Ding, J., Zhang, W., and Wang, X., 2010, "Tribological Behaviors of Graphite/Epoxy Two-Phase Composite Coatings," Tribol. Int., **43**(8), pp. 1318–1325.
[30] Wang, C., Wang, H., Li, M., Liu, Z., Lv, C., Zhu, Y., and Bao, N., 2018, "Anti-Corrosion and Wear Resistance Properties of Polymer Composite Coatings: Effect of Oily Functional Fillers," J. Taiwan Inst. Chem. Eng., **85**, pp. 248–256.
[31] Mohan, T., and Kanny, K., 2019, "Tribological Properties of Nanoclay-Infused Banana Fiber Reinforced Epoxy Composites," ASME J. Tribol., **141**(5), p. 052003.
[32] Gafsi, N., Smaoui, I., Verdejo, R., Kharrat, M., Manchado, MÁ, and Dammak, M., 2021, "Tribological and Mechanical Characterization of Epoxy/Graphite Composite Coatings: Effects of Particles' Size and Oxidation," Proc. Inst. Mech. Eng. J, **235**(1), pp. 129–137.
[33] Surnam, B. Y. R., Chui, C.-W., Xiao, H., and Liang, H., 2016, "Investigating Atmospheric Corrosion Behavior of Carbon Steel in Coastal Regions of Mauritius Using Raman Spectroscopy," Matéria (Rio J.), **21**(1), pp. 157–168.
[34] Surnam, B., Chiu, C., Xiao, H., and Liang, H., 2015, "Long Term Atmospheric Corrosion in Mauritius," Corros. Eng., Sci. Technol., **50**(2), pp. 155–159.
[35] Akinci, A., 2009, "The Salt Spray Corrosion of Polymer Coating on Steel," Arab. J. Sci. Eng., **34**, p. 139.
[36] Chen, X., Yang, H. Y., Abbott, T., Easton, M. A., and Birbilis, N., 2012, "Corrosion-Resistant Electrochemical Platings on Magnesium Alloys: A State-of-the-Art Review," Corrosion, **68**(6), pp. 518–535.
[37] De Damborenea, J., Conde, A., and Arenas, M., 2014, "Corrosion Inhibition With Rare Earth Metal Compounds in Aqueous Solutions," *Rare Earth-Based Corrosion Inhibitors*, Elsevier, New York, pp. 84–116.
[38] Monticelli, C., 2018, *Encyclopedia of Interfacial Chemistry*, Elsevier, University of Ferrara, Ferrara, Italy, pp. 164–171.
[39] Bahlakeh, G., Ramezanzadeh, B., Dehghani, A., and Ramezanzadeh, M., 2019, "Novel Cost-Effective and High-Performance Green Inhibitor Based on Aqueous *Peganum harmala* Seed Extract for Mild Steel Corrosion in HCl Solution: Detailed Experimental and Electronic/Atomic Level Computational Explorations," J. Mol. Liq., **283**, pp. 174–195.
[40] Obot, I., Meroufel, A., Onyeachu, I. B., Alenazi, A., and Sorour, A. A., 2019, "Corrosion Inhibitors for Acid Cleaning of Desalination Heat Exchangers: Progress, Challenges and Future Perspectives," J. Mol. Liq., **296**, p. 111760.
[41] Yu, Y., Shironita, S., Souma, K., and Umeda, M., 2018, "Effect of Chromium Content on the Corrosion Resistance of Ferritic Stainless Steels in Sulfuric Acid Solution," Heliyon, **4**(11), p. e00958.
[42] Kim, J. K., Kim, Y. H., Lee, J. S., and Kim, K. Y., 2010, "Effect of Chromium Content on Intergranular Corrosion and Precipitation of Ti-Stabilized Ferritic Stainless Steels," Corros. Sci., **52**(5), pp. 1847–1852.
[43] Kamimura, T., and Stratmann, M., 2001, "The Influence of Chromium on the Atmospheric Corrosion of Steel," Corros. Sci., **43**(3), pp. 429–447.
[44] Denpo, K., and Ogawa, H., 1993, "Effects of Nickel and Chromium on Corrosion Rate of Linepipe Steel," Corros. Sci., **35**(1–4), pp. 285–288.
[45] Husby, H., Iannuzzi, M., Johnsen, R., Kappes, M., and Barnoush, A., 2018, "Effect of Nickel on Hydrogen Permeation in Ferritic/Pearlitic Low Alloy Steels," Int. J. Hydrogen Energy, **43**(7), pp. 3845–3861.
[46] Tian, Y., Dong, C., Wang, G., Cheng, X., and Li, X., 2020, "The Effect of Nickel on Corrosion Behaviour of High-Strength Low Alloy Steel Rebar in Simulated Concrete Pore Solution," Constr. Build. Mater., **246**, p. 118462.
[47] Cheng, X., Jin, Z., Liu, M., and Li, X., 2017, "Optimizing the Nickel Content in Weathering Steels to Enhance Their Corrosion Resistance in Acidic Atmospheres," Corros. Sci., **115**, pp. 135–142.
[48] Alamri, H., Al-Shahrani, A., Bovero, E., Khaldi, T., Alabedi, G., Obaid, W., Al-Taie, I., and Fihri, A., 2018, "Self-Cleaning Superhydrophobic Epoxy Coating Based on Fibrous Silica-Coated Iron Oxide Magnetic Nanoparticles," J. Colloid Interface Sci., **513**, pp. 349–356.
[49] Šolić, T., Marić, D., Putnik, I., and Samardžić, I., 2019, "Corrosion Resistance of the X6CrNiTi18-10 Material Exposed to a Salt Spray Test," Metallurgy, **58**(3–4), pp. 307–310.
[50] Grassini, S., Matteis, P., Scavino, G., Rossetto, M., and Firrao, D., 2011, "Salt Spray Corrosion of Mechanical Junctions of Magnesium Castings," Magnesium Technol., **2011**, pp. 493–499.
[51] Huang, N., Jin, N., and Luo, X.-F., 2016, "Influence of Salt Spray Environment on the Transmission Characteristics of the Dual Left-Handed Material," Prog. Electromagn. Res. Lett., **63**, pp. 129–134.
[52] Varacalle Jr, D., Zeek, D., Couch, K., Benson, D., and Kirk, S., 1997, *Flame Spraying of Polymers*, Lockheed Martin Idaho Technologies Co., Idaho National Engineering Lab, Idaho Falls, ID.
[53] Nunes, R. A. X., Costa, V. C., Calado, V. M. d. A., and Branco, J. R. T., 2009, "Wear, Friction, and Microhardness of a Thermal Sprayed PET: Poly (Ethylene Terephthalate) Coating," Mater. Res., **12**(2), pp. 121–125.
[54] Lorenz, W., and Mansfeld, F., 1981, "Determination of Corrosion Rates by Electrochemical DC and AC Methods," Corros. Sci., **21**(9–10), pp. 647–672.
[55] Jha, S., Chen, Y., Wang, R., Gharib, M., and Liang, H., 2019, "Design and Synthesis of a High Performance Coating," American Society of Mechanical Engineers, Salt Lake City, UT, Nov. 11–14, p. V012T10A044.
[56] Nowicki, B., 1985, "Multiparameter Representation of Surface Roughness," Wear, **102**(3), pp. 161–176.
[57] Whitley, J., Kusy, R., Mayhew, M., and Buckthal, J., 1987, "Surface Roughness of Stainless Steel and Electroformed Nickel Standards Using a HeNe Laser," Opt. Laser Technol., **19**(4), pp. 189–196.
[58] Song, W., Gu, A., Liang, G., and Yuan, L., 2011, "Effect of the Surface Roughness on Interfacial Properties of Carbon Fibers Reinforced Epoxy Resin Composites," Appl. Surf. Sci., **257**(9), pp. 4069–4074.
[59] Liu, D., Zhao, W., Liu, S., Cen, Q., and Xue, Q., 2016, "Comparative Tribological and Corrosion Resistance Properties of Epoxy Composite Coatings Reinforced With Functionalized Fullerene C60 and Graphene," Surf. Coat. Technol., **286**, pp. 354–364.
[60] Joly-Pottuz, L., Dassenoy, F., Martin, J., Vrbanic, D., Mrzel, A., Mihailovic, D., Vogel, W., and Montagnac, G., 2005, "Tribological Properties of Mo–S–I Nanowires as Additive in Oil," Trib. Lett., **18**(3), pp. 385–393.
[61] Meng, F., Zhang, Z., Gao, P., Kang, R., Boyjoo, Y., Yu, J., and Liu, T., 2020, "Excellent Tribological Properties of Epoxy—Ti3C2 With Three-Dimensional Nanosheets Composites," Friction, **9**(4), pp. 1–13.
[62] Yan, H., Li, W., Li, H., Fan, X., and Zhu, M., 2019, "Ti3C2 MXene Nanosheets Toward High-Performance Corrosion Inhibitor for Epoxy Coating," Prog. Org. Coat., **135**, pp. 156–167.
[63] Hou, X., Shan, C., and Choy, K.-L., 2008, "Microstructures and Tribological Properties of PEEK-Based Nanocomposite Coatings Incorporating Inorganic Fullerene-Like Nanoparticles," Surf. Coat. Technol., **202**(11), pp. 2287–2291.
[64] Zhang, G., Liao, H., Li, H., Mateus, C., Bordes, J.-M., and Coddet, C., 2006, "On Dry Sliding Friction and Wear Behaviour of PEEK and PEEK/SiC-Composite Coatings," Wear, **260**(6), pp. 594–600.
[65] Verma, C., Olasunkanmi, L. O., Akpan, E. D., Quraishi, M., Dagdag, O., El Gouri, M., Sherif, E.-S. M., and Ebenso, E. E., 2020, "Epoxy Resins as Anticorrosive Polymeric Materials: A Review," React. Funct. Polym., **156**, p. 104741.
[66] Le Pen, C., Lacabanne, C., and Pébère, N., 2000, "Structure of Waterborne Coatings by Electrochemical Impedance Spectroscopy and a Thermostimulated Current Method: Influence of Fillers," Prog. Org. Coat., **39**(2–4), pp. 167–175.
[67] Veleva, L., Chin, J., and Del Amo, B., 1999, "Corrosion Electrochemical Behavior of Epoxy Anticorrosive Paints Based on Zinc Molybdenum Phosphate and Zinc Oxide," Prog. Org. Coat., **36**(4), pp. 211–216.
[68] Vilche, J., Bucharsky, E., and Giudice, C. A., 2002, "Application of EIS and SEM to Evaluate the Influence of Pigment Shape and Content in ZRP Formulations on the Corrosion Prevention of Naval Steel," Corros. Sci., **44**(6), pp. 1287–1309.
[69] Bierwagen, G., Battocchi, D., Simões, A., Stamness, A., and Tallman, D., 2007, "The Use of Multiple Electrochemical Techniques to Characterize Mg-Rich Primers for Al Alloys," Prog. Org. Coat., **59**(3), pp. 172–178.
[70] Bayram, T. C., Orbey, N., Adhikari, R. Y., and Tuominen, M., 2015, "FP-Based Formulations as Protective Coatings in Oil/Gas Pipelines," Prog. Org. Coat., **88**, pp. 54–63.
[71] Tang, G., Zhang, K., Yan, Z., Ma, L., and Huang, X., 2017, "A Self-Curing, Thermosetting Resin Based on Epoxy and Organic Titanium Chelate as an Anticorrosive Coating Matrix for Heat Exchangers: Preparation and Properties," Prog. Org. Coat., **102**, pp. 225–230.
[72] Lam, C. K., and Lau, K. T., 2006, "Localized Elastic Modulus Distribution of Nanoclay/Epoxy Composites by Using Nanoindentation," Compos. Struct., **75**(1–4), pp. 553–558.
[73] Shi, G., Zhang, M. Q., Rong, M. Z., Wetzel, B., and Friedrich, K., 2003, "Friction and Wear of Low Nanometer Si3N4 Filled Epoxy Composites," Wear, **254**(7–8), pp. 784–796.